Contents

Supplemental Table 1. Fractionation factors 44-40 Ca calcite-dissolved

$\Delta^{44}Ca$	$\alpha^{44}Ca$	Example	reference
-0.66	0.99934	White Moon Cave modern calcite; slow growth rate experimental	(de Wet et al., 2021; Mills et al., 2021; Tang et al., 2008)
-0.86	0.99914		
-1.08	0.99892		
-1.37	0.99863	Heshang Cave modern calcite; fast growth rate experimental	(Mills et al., 2021; Owen et al., 2016; Tang et al., 2008)

Supplemental Table 2. Age constraints for stalagmites. For BEL, GLD, and ROW

Sample ID	^{238}U (ppb)		^{232}Th (ppt)		^{230}Th / ^{232}Th (atomic x10^{-6})		$d^{234}U$* (measured)		^{230}Th / ^{238}U (activity)		^{230}Th Age (yr) (uncorrected)		^{230}Th Age (yr) (corrected)		$d^{234}U_{initial}$** (corrected)		^{230}Th Age (yr BP)*** (corrected)		mm from tip
GLD 60	1221.8	±1.8	34	±1	348121	±14453	-13.2	±1.2	0.5892	±0.0015	99411	±461	**99410**	**±461**	-17	±2	**99339**	**±461**	17.0
GLD																	**111000***		91.0
GLD																	**133000***		173.0
GLD																	**185000***		185.0
GLD 243	839.2	±1.2	1061	±21	9823	±198	32.8	±1.4	0.7531	±0.0017	140840	±785	**140805**	**±785**	49	±2	**140734**	**±785**	199.0
ROW43	1518.6	±2.0	90	±2	170667	±4575	-17.8	±1.2	0.6118	±0.0011	106786	±400	**106784**	**±400**	-24	±2	**106715**	**±400**	420
ROW-20	1303.4	±1.7	285	±6	40397	±894	6.3	±1.5	0.5353	±0.0010	82690	±309	**82683**	**±309**	8	±2	**82612**	**±309**	20
ROW-105	1668.2	±1.7	212	±6	73666	±2144	-3.2	±1.2	0.5683	±0.0008	92117	±287	**92113**	**±287**	-4	±2	**92042**	**±287**	105
ROW-260/280	1678.6	±1.7	147	±4	109562	±3083	-21.4	±1.1	0.5818	±0.0008	98891	±300	**98888**	**±300**	-28	±1	**98817**	**±300**	260
BEL5	2358.2	±3.7	433	±9	57092	±1169	-68.7	±1.2	0.6358	±0.0013	128083	±621	**128077**	**±621**	-99	±2	**128008**	**±621**	54.0
BEL 160	896.6	±0.7	12	±2	776228	±151042	-53.0	±1.2	0.6551	±0.0009	130683	±524	**130683**	**±524**	-77	±2	**130612**	**±524**	160.0
BEL 210	1030.0	±0.9	16	±1	707178	±53512	-55.9	±1.2	0.6615	±0.0008	134172	±521	**134171**	**±521**	-82	±2	**134100**	**±521**	210.0

* based on tiepoints of $\delta^{18}O$ with GAR record of Stoll et al., 2022

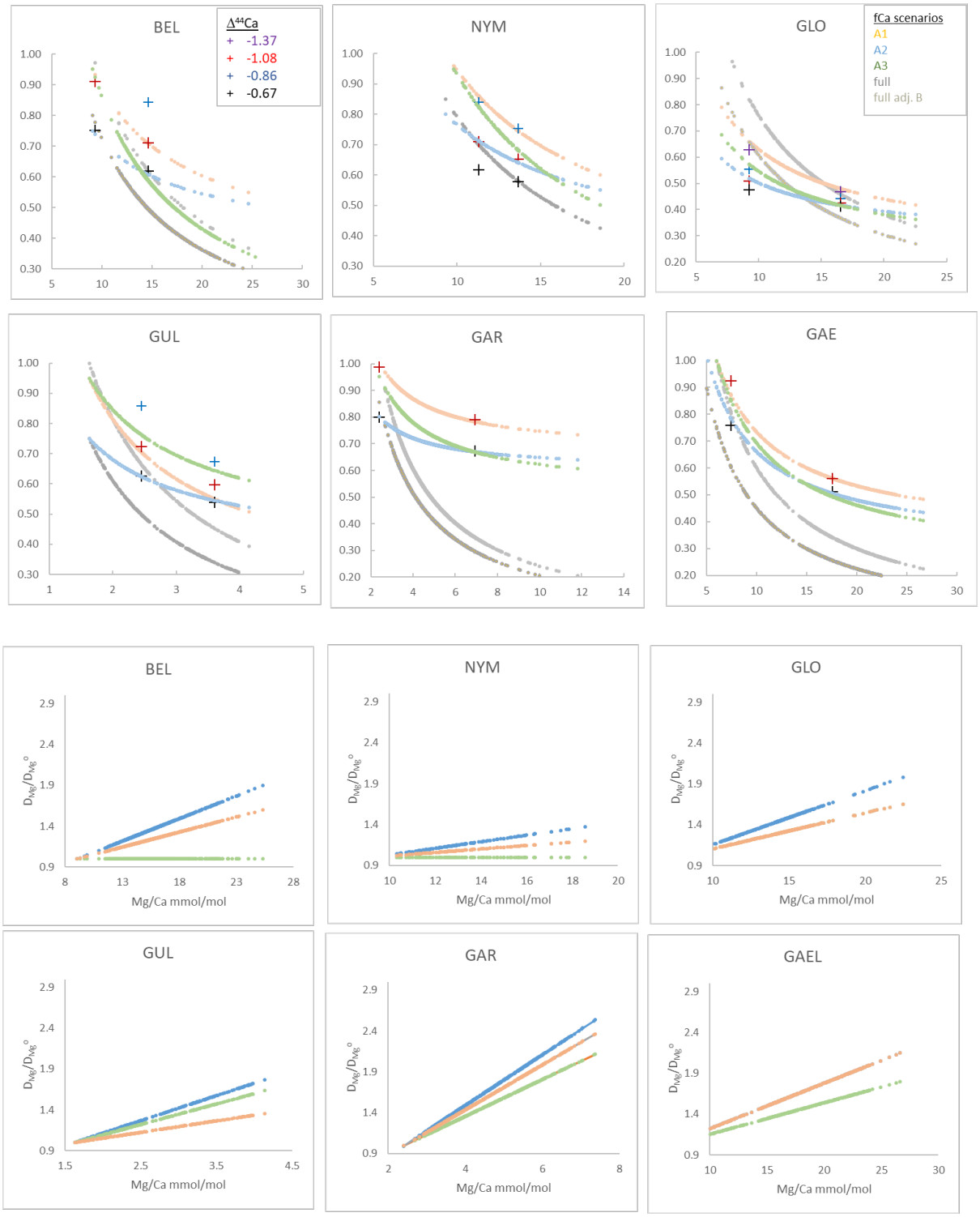

Supplemental Figure 1. fCa vs measured Mg/Ca as Figure 5. Crosses show fCa calculated from $d^{44}Ca$ according to different $\Delta^{44}Ca$ fractionation factor Gray curves show calculation of fCa from Mg/Ca assuming Mg/Ca_{min} reflects undegassed dripwater (upper gray line) or that undegassed dripwater is lower than minimum Mg/Ca by factor from 0.65 to 0.95 (lower gray line; value in Supplemental Table 1). Pink, blue,and green lines illustrate scenarios A1, A2, and A3 which are potential relationships between fCa and Mg/Ca consistent with $\delta^{44}Ca$ fCa estimates according to Equation 7 and fit parameters in Table2. c)-d) The variation in DMg implied by scenarios in a)-b),calculated as in Equation 8 and assuming constant congruent bedrock dissolution to yield a constant initial undegassed Mg/Ca ratio of dripwater. A 10°C temperature increase would cause D/D_o to reach 1.22 according to laboratory experiments(Day and Henderson, 2013).

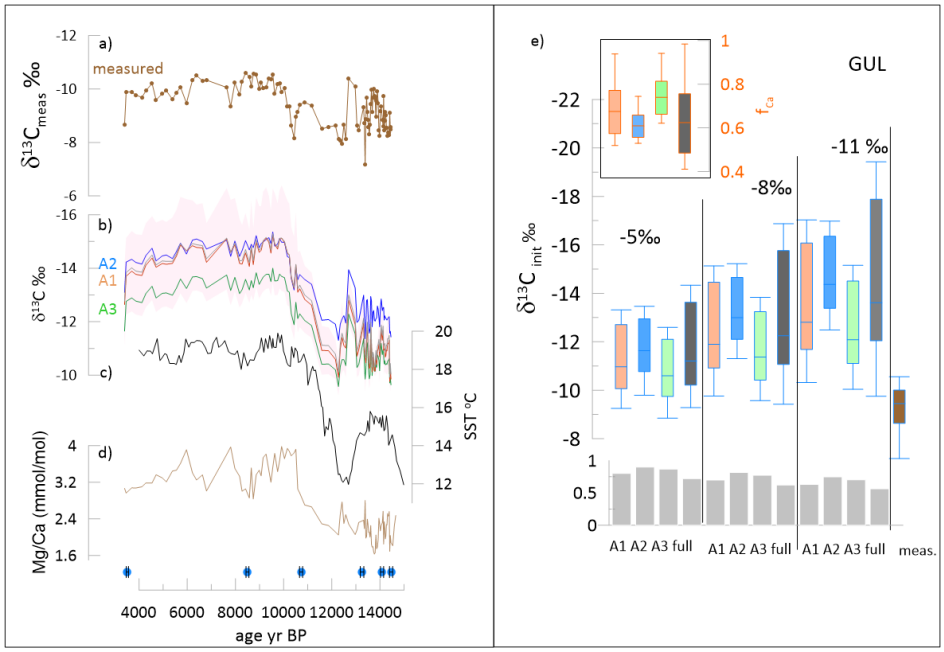

Supplementary Figure 2. Full time series and statistics for Holocene stalagmite GUL. Supplementary Figure 2. Full time series and statistics for Holocene stalagmite GAL. Left panel shows the measured $\delta^{13}C$ and the $\delta^{13}C_{init}$ for three fCa scenarios; the line shows the result for degassing fractionation slope of -8 ‰, and shading for the A3 scenario shows the range using other degassing slopes of -5 ‰ (more positive), and -11 ‰ (more negative). Right panel, inset shows the median and range of fCa for the various scenarios. Box and whisker plot shows the median, upper and lower quartile, and 1/99% ranges for the calculated $\delta^{13}C_{init}$ for each of the fCa scenarios (color coded as in Table 2 and Figure 5) and the measured $\delta^{13}C$. Gray bars at the base of each figure illustrate the Pearson correlation coefficient between the $\delta^{13}C_{init}$ and the measured $\delta^{13}C_{init}$.

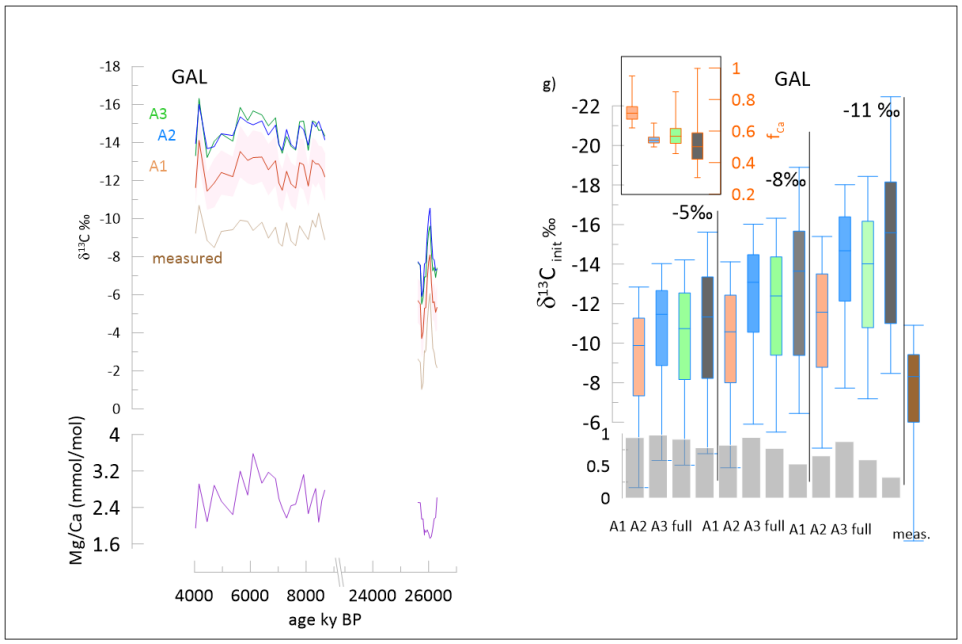

Supplementary Figure 3. Full time series and statistics for Holocene stalagmite GAL. Left panel shows the measured $\delta^{13}C$ and the $\delta^{13}C_{init}$ for three fCa scenarios; the line shows the result for degassing fractionation slope of -8 ‰, and shading for the A3 scenario shows the range using other degassing slopes of -5 ‰ (more positive), and -11 ‰ (more negative). Right panel, inset shows the median and range of fCa for the various scenarios as in Supplemental Figure 2.

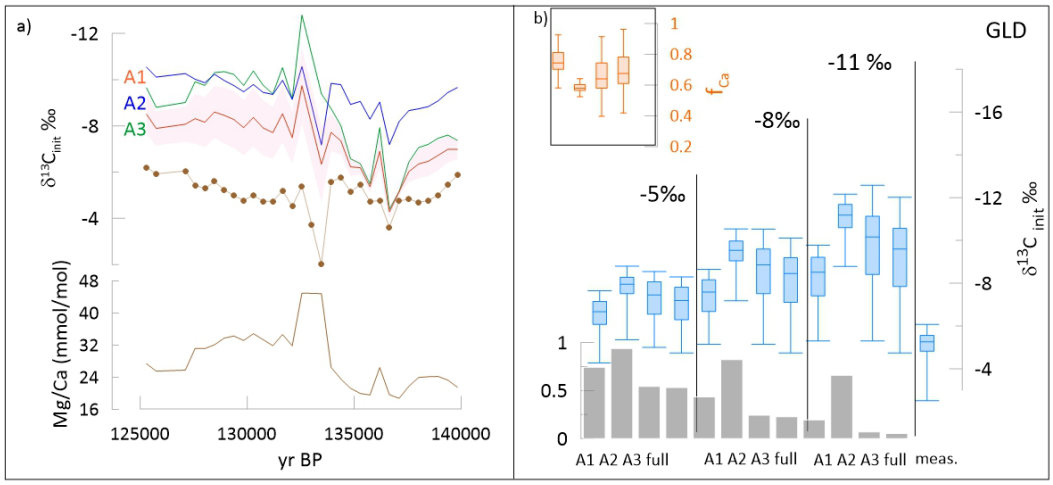

Supplementary Figure 4. Full time series and statistics for stalagmite GLD. Left panel shows the measured $\delta^{13}C$ and the $\delta^{13}C_{init}$ for three fCa scenarios; the line shows the result for degassing fractionation slope of -8 ‰, and shading for the A3 scenario shows the range using other degassing slopes of -5 ‰ (more positive), and -11 ‰ (more negative). Right panel, inset shows the median and range of fCa for the various scenarios as in Supplemental Figure 2.

Supplementary discussion on the potential role of non-bedrock Mg in this cave system

We have used I-STAL to investigate effects of changing seawater aerosol fluxes on stalagmite Mg/Ca ratios, assuming dripwater Na is entirely marine sourced and contributes marine Mg according to seawater Mg/Na ratio. Modern dripwater studies show Na concentrations of 5 ppm (Kost et al., in review).

Systematic variation in the relative contribution of bedrock Mg and Mg input from non-bedrock sources, such as marine aerosols, exerts only limited influence on the initial Mg/Ca of undegassed dripwater in this system. Aerosol monitoring studies show that the aerosol delivery at these distances from the coast is insensitive to increased distance from the coast, such as the up to 4 km additional distance at glacial sea level minima(Meira et al., 2007; Meira et al., 2006). Even for the stalagmites fed by lowest bedrock Mg/Ca, reduction in the degree of bedrock dissolution (eg from 105 to 60 ppm Ca), with constant modern rates of aerosol delivery, would lead to only modest increase in the estimated fCa by about 10%, much smaller than the up to 2-fold amplification observed for many stalagmites. Rather, if Mg partitioning were varying only in the range expected due to temperature dependence, stalagmites fed by such bedrock sources would require a 4-fold increase in delivery of non-bedrock Mg sources to generate the observed amplification of Mg/Ca with respect to δ^{44}Ca. For stalagmites fed by the intermediate Mg bedrock (eg GAR), a 7-fold increase in delivery of non-bedrock Mg sources would be required to generate the observed amplification of Mg/Ca with respect to δ^{44}Ca. These would reflect rather dramatic changes in external fluxes which must also be systematically related to the PCP and thereby correlate with δ^{44}Ca. While such a correlation cannot be ruled out on the basis of current data. a systematic correlation between DMg and Mg/Ca is a more straightforward mechanism for the observed amplification. A larger dataset of paired δ^{44}Ca and Mg/Ca for a given stalagmite, coupled with assessment of changes in fluid inclusion density, would be useful to further test the factors responsible for inferred apparent variation in DMg.

References

Day, C.C., Henderson, G.M., 2013. Controls on trace-element partitioning in cave-analogue calcite. Geochimica et Cosmochimica Acta 120, 612-627.
de Wet, C.B., Erhardt, A.M., Sharp, W.D., Marks, N.E., Bradbury, H.J., Turchyn, A.V., Xu, Y., Oster, J.L., 2021. Semiquantitative estimates of rainfall variability during the 8.2 kyr event in California using speleothem calcium isotope ratios. Geophysical Research Letters 48, e2020GL089154.
Meira, G., Andrade, C., Alonso, C., Padaratz, I., Borba Jr, J., 2007. Salinity of marine aerosols in a Brazilian coastal area—Influence of wind regime. Atmospheric Environment 41, 8431-8441.
Meira, G., Andrade, M., Padaratz, I., Alonso, M., Borba Jr, J., 2006. Measurements and modelling of marine salt transportation and deposition in a tropical region in Brazil. Atmospheric Environment 40, 5596-5607.
Mills, J.V., DePaolo, D.J., Lammers, L.N., 2021. The influence of Ca: CO3 stoichiometry on Ca isotope fractionation: Implications for process-based models of calcite growth. Geochimica et Cosmochimica Acta 298, 87-111.
Owen, R., Day, C., Hu, C.-Y., Liu, Y.-H., Pointing, M., Blättler, C., Henderson, G., 2016. Calcium isotopes in caves as a proxy for aridity: Modern calibration and application to the 8.2 kyr event. Earth and Planetary Science Letters 443, 129-138.
Tang, J., Dietzel, M., Böhm, F., Köhler, S.J., Eisenhauer, A., 2008. Sr2+/Ca2+ and 44Ca/40Ca fractionation during inorganic calcite formation: II. Ca isotopes. Geochimica et Cosmochimica Acta 72, 3733-3745.